

1 **A framework for ^{210}Pb model selection and its application to 37 cores from Eastern Canada to identify**
2 **the dynamics and drivers of lake sedimentation rates**

3
4 Alexandre Baud^{1,2,3}, Candice Aulard^{3,4}, Hamid Ghanbari^{3,5}, Maxime Fradette⁶, Dermot Antoniadis^{3,5}, Paul
5 del Giorgio^{3,4}, Yannick Huot^{3,5}, Pierre Francus^{2,7}, John Smol⁸ and Irene Gregory-Eaves^{1,3}

6
7 ¹Biology Department, McGill University, Montréal, Québec, H3A 1B1, Canada

8 ²Centre Eau Terre Environnement, Institut National de la Recherche Scientifique (INRS), Québec City,
9 Québec, G1K 9A9, Canada

10 ³Group for Interuniversity Research in Limnology and Aquatic Environments (GRIL);

11 ⁴Département des sciences biologiques, Université du Québec à Montréal, Montréal, Québec, H2X 3X8,
12 Canada

13 ⁵Département de géographie, Université Laval, Québec City, Québec G1V 0A6, Canada

14 ⁶Département de géomatique appliquée, Université de Sherbrooke, Sherbrooke, Québec, J1K 2R1

15 ⁷GEOTOP, Geochemistry and Geodynamics Research Centre, Université du Québec à Montréal,
16 Montréal, Québec H3C 3P8, Canada

17 ⁸Biology Department, Queen's University, Kingston, Ontario, K7L 3N6, Canada

18

19 **Corresponding author:**

20 Alexandre Baud,
21 Biology Department, McGill University,
22 Montréal, Québec, H3A 1B1, Canada

23

24 **Telephone:** +1 (514) 398 4119

25 **Email:** alexandre.baud@mail.mcgill.ca

26

27

28

29

30

31 Abstract

32 Lake sedimentation rate represents a synthetic metric of ecosystem functioning. Many localized studies
33 have reported a significant association between land use/land cover changes and lake sediment mass
34 accumulation rates, with a few global syntheses echoing these findings at larger scales. In the literature,
35 studies evaluating lead-210 (^{210}Pb) for establishing sediment chronologies will report at least one of
36 three dating models, but the constant rate of supply (C.R.S.) model is the most widely used. However, it
37 is often unclear how or why this model is selected, despite its influence on the interpretation of many
38 subsequent analyses about ecosystem dynamics and functioning. It would thus be advantageous to
39 design an objective and semi-automated way of choosing among dating models. We measured
40 radioisotopic activities in 37 sediment cores across four ecozones of eastern Canada and developed an
41 approach to assess model fit for the three commonly applied dating models. The derived chronologies
42 were then used to evaluate the spatial and temporal variation in sedimentation rates across four
43 ecozones in Canada (covering a surface area of $2.2 \times 10^6 \text{ km}^2$). We observed a recent increase in lake
44 sedimentation rates across most lakes, as has been observed globally, albeit with significant differences
45 in the magnitude of sedimentation rates across ecozones. Across all lakes, we found that regional
46 human population counts and mean annual air temperatures were significant temporal predictors of
47 variation in mass accumulation rates. Overall, this analytical framework offers an objective approach for
48 assessing fit and selecting among sediment age models, which contributes to a more robust
49 quantification of sedimentation rates. With this first application, we provide a quantitative assessment
50 of how lake sedimentation rates vary across a northern lake-rich region and have responded to
51 environmental change.

52

53 **Keywords:** Radiochronology, ^{210}Pb , Dating Models, C.R.S., C.I.C., C.F.C.S., Paleolimnology, Sedimentation
54 Rates, Land-use

55

56

57 Introduction

58 Lakes are critical ecosystems, acting as hotspots of biogeochemical cycling and biodiversity
59 (Schallenberg et al., 2013). Using proxies of past conditions preserved in lake sediments,
60 paleolimnologists can reconstruct shifts in lake ecosystem properties and of their surrounding
61 watersheds, on scales spanning decades to millennia (Last et al., 2003; Korosi et al., 2013). While
62 paleolimnology can provide insights and context for local and regional environmental changes over
63 extended timescales, the study of lake sediment cores also provides key insights into ecosystem
64 functioning (Millet et al., 2010; Winegardner et al., 2017). In particular lake sediment mass accumulation
65 rates (MAR) are reflective of both the export of materials from the watershed and of material processing
66 and burial within lakes, and in turn strongly influence the biogeochemical functioning of lakes. Several
67 authors have recently evaluated the temporal change in lake sedimentation regimes and the factors
68 controlling them across large regions. For example, sedimentation rates have increased globally during
69 the mid to late Holocene, coincident with forest clearance and the onset of European-style agriculture
70 (Jenny et al., 2016). Considering a more recent time frame, Baud et al. (2021) found global

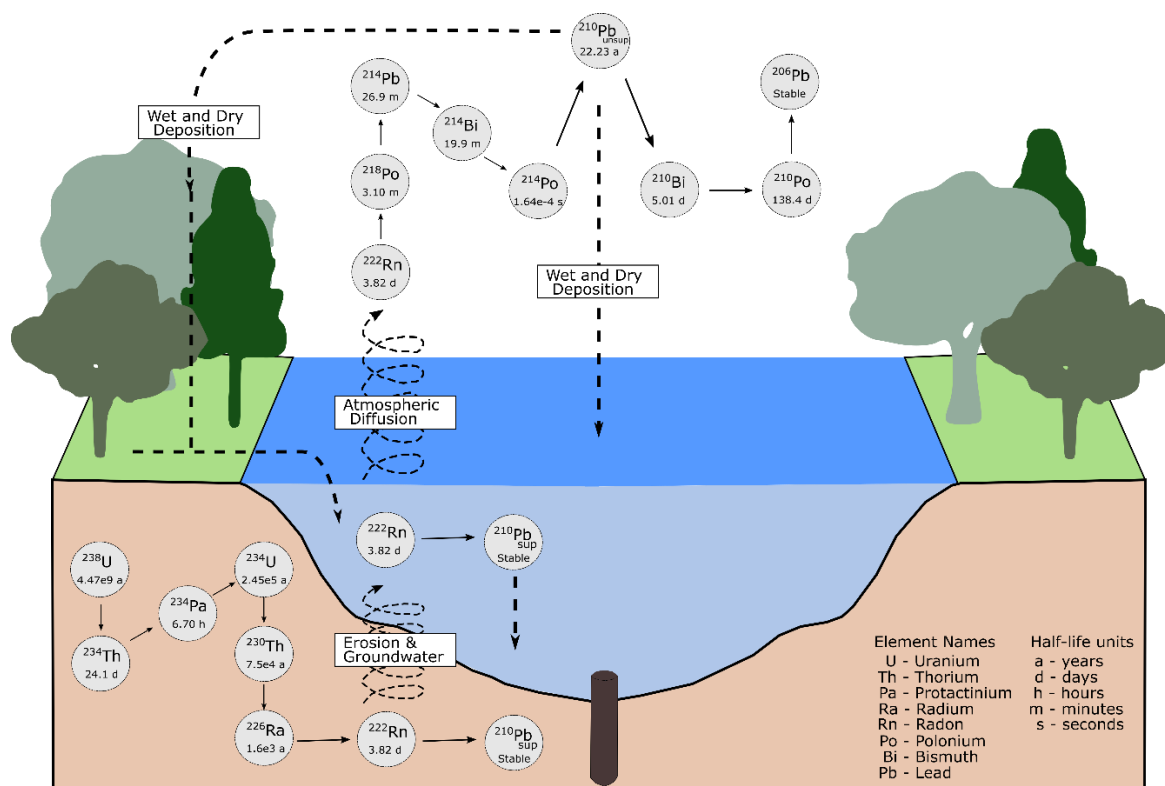
71 sedimentation rates to have increased 3- to 4-fold since ca. 1850 CE, associated with further expansion
72 of agriculture and urbanization.

73 The development of reliable sediment chronologies is critical to establishing sedimentation rates, which
74 in absence of annual laminae (i.e., varves) are most often derived through the quantification and
75 analysis of naturally occurring radioisotopes, such as radioisotopic lead (^{210}Pb) for recent sediments.
76 ^{210}Pb has a half-life of 22.23 years (DDEP, 2010), and thus is an obvious candidate for the chronological
77 dating of recent sediments. While the account of the lead radioisotopic decay series has been described
78 elsewhere (Goldberg, 1963; Krishnaswami, 1978; Appleby and Oldfield, 1983), it is important to note
79 that radioactive lead is part of the natural decay series of uranium. ^{210}Pb activities in sediment records
80 originate from two components: 1) a supported ^{210}Pb component, derived from the in situ radioactive
81 decay series of uranium-238 (^{238}U) in soils and from the transfer of radon-222 (^{222}Rn) via surface run-off
82 or groundwater contribution; and 2) an unsupported ^{210}Pb fraction, derived from ^{222}Rn that first diffuses
83 from the Earth's surface into the atmosphere and subsequently decays into ^{210}Pb (Ghaleb, 2009) (Figure
84 1). This unsupported ^{210}Pb component is expected to follow a first order-decay rate while the supported
85 ^{210}Pb component is expected to have a constant, near-zero activity. The supported ^{210}Pb fraction is often
86 measured via gamma spectroscopy by quantifying the activity of short-lived daughter products of
87 radium-226 (^{226}Ra) such as lead-214 (^{214}Pb) or bismuth-214 (^{214}Bi) (Martz et al., 1991). With gamma
88 spectroscopy, additional radioisotopes independent of the ^{210}Pb decay series are routinely measured,
89 providing validation for ^{210}Pb dating methods. These radioisotopes include cesium-137 (^{137}Cs) and
90 americium-241 (^{241}Am), both of which are associated with radioactive fallout. Cesium-137 is expected to
91 begin rising in the sedimentary record around 1950, when the first nuclear weapons tests were initiated,
92 and reach peak activities ca. 1963 CE (Pennington et al., 1976), the year of maximum atmospheric
93 nuclear testing (Wright et al., 1999). Likewise, ^{241}Am has been reported to reach maximum abundance
94 around 1963 (Appleby et al., 1991). The meltdown of the Chernobyl reactors (1986 CE) created a second
95 peak in ^{137}Cs , mainly over northern Europe.

96

97

98



99

100 **Figure 1.** The ^{238}U (uranium) decay series accounting for the deposition of supported ^{210}Pb and
 101 unsupported ^{210}Pb into lake sediments via wet and dry deposition on the landscape. Solid lines
 102 represent the radionuclide transitions while curved dashed lines account for the transfer of ^{222}Rn from
 103 the lithosphere into lakes via erosion and from lakes into the atmosphere via diffusion.

104

105 Stemming from the behavior of the measured ^{210}Pb activity in sediment cores, different dating models
 106 have emerged, each with different assumptions and applications. There are three main models: the
 107 Constant Flux Constant Sedimentation model (C.F.C.S.); the Constant Initial Concentration model (C.I.C.);
 108 and the Constant Rate of Supply model (C.R.S.). All three models have a central assumption of an
 109 unmixed temporal structure of the sediment core where the ^{210}Pb incorporated within it follows its
 110 natural accumulated order and is not affected by any subsequent redistribution processes. However, the
 111 three models differ in the fraction of ^{210}Pb investigated and its expected decay function, thereby yielding
 112 divergent age models (Table 1). The choice of model therefore has implications for the estimates of the
 113 age of individual sediment layers, but perhaps more importantly, may greatly influence not only the
 114 sediment mass accumulation rates that are derived from these modeled ages, but also any assessment
 115 of potential changes in these accumulation rates that may have occurred over past decades, the latter
 116 being a fundamental and yet unresolved issue in contemporary limnology.

117 When confronted with the outputs from the three dating models for any one sediment core, selecting
 118 the model that best reflects the core chronology is not a straightforward procedure. An in-depth
 119 evaluation of the sediment properties and possible changes in the sediment stratigraphy, the lake and
 120 its watershed and airshed as well as a clear account of historical events (human settlement, known flood

121 events) are often necessary to gain full confidence in the derived chronology. This knowledge, which is
 122 also clearly useful for more than just developing a chronology, can be difficult to obtain, especially when
 123 considering large numbers of lakes or sites in remote regions. When dealing with model selection,
 124 previous regional coring efforts have used independent markers to validate the derived ^{210}Pb -based
 125 chronology, including other radioisotopes (e.g., ^{137}Cs and ^{241}Am), modern contaminants, forest fires or
 126 pollen markers indicative of recent settlement activities (e.g., the *Ambrosia* rise in eastern North
 127 America) (Blais et al., 1995; Smol, 2008).

128 Most commonly, only peak activities of ^{137}Cs and (more rarely) ^{241}Am are considered when evaluating
 129 ^{210}Pb -based chronologies. Given that gamma spectroscopy measures these radioisotopes at the same
 130 time as ^{210}Pb activities, many investigators have easy access to these data. Most studies publishing ^{210}Pb
 131 profiles measured from gamma spectroscopy will report the use of ^{137}Cs (Turner and Delorme, 1996).
 132 However, several papers have emerged over the past few decades highlighting the potential for post-
 133 depositional mobility of ^{137}Cs (Davis et al., 1984; Klaminder et al., 2012). Unfortunately, other
 134 independent measures can require extensive laboratory processing, or are simply not possible due to
 135 shortages of sediment material.

136 Based on several large, regional paleolimnological studies, a few key observations regarding sediment
 137 dating have emerged. For example, in a study of ~30 North American lakes, Binford et al. (1993)
 138 compared chronologies derived from the C.I.C. and C.R.S. models with multiple independent markers
 139 (^{137}Cs , fly ash, and the *Ambrosia* rise were analyzed in cores from Florida, New-England Adirondack
 140 Mountains and Minnesota). While the authors reported having considered both dating models, they
 141 later state that they relied exclusively on C.R.S.-derived ages. This choice was mainly motivated by the
 142 fact that previous studies had reported variable sedimentation rates and dilution of the ^{210}Pb in surficial
 143 sediment by higher sediment accumulation rates (Binford and Brenner 1986). In another study of 22
 144 lake sediment cores from the Canadian Prairies, Turner and Delorme (1996) also considered multiple
 145 dating models and generally observed a good agreement (in over 50% of the cores) between the dates
 146 derived from C.I.C and C.R.S. models. Having validated their chronologies using ragweed (*Ambrosia*)
 147 pollen, the authors also noted that, in some instances, the close agreement in core chronologies
 148 between models only held true for the upper most (recent) section of the sediment cores, beyond which
 149 the C.R.S. model started to assign much older dates as a function of small increases in core depth. This
 150 account of age over-estimation of the C.R.S. model in deeper sediments was also noted in more recent
 151 work (Bruel and Sabatier, 2020). It is thus recommended to be careful or to avoid extrapolating C.R.S.
 152 age models beyond the point where the ^{210}Pb inventory has reached background activity. As reported
 153 from a global synthesis of published sediment chronologies from the *Journal of Paleolimnology*, the
 154 C.R.S. model was the most popular dating model, being reported in over 75% of the studies establishing
 155 recent sediment radiochronology (Baud et al., 2021).

156 In this study, we have explicitly applied and compared the three dating models to radioisotopic
 157 sediment profiles for 37 lakes spanning four ecozones of eastern Canada to develop a robust and
 158 consistent framework for the selection of lake sediment age models. We then applied the resulting
 159 framework to estimate mass sedimentation rates for these lakes, to assess both cross lake patterns in
 160 sedimentation and potential temporal shifts in these rates. Given the substantial differences in land use,
 161 vegetation and climate across these ecozones, we expected both differences in mean mass
 162 sedimentation rates as well as variation in recent sediment mass accumulation rates among ecozones.
 163 Furthermore, given that human population and land use have emerged as significant predictors of

164 sedimentation rates in a global database (Baud et al., 2021), we tested the hypothesis that catchment-
165 scale human population would be a significant predictor of sedimentation rates across time and among
166 lakes in our four Canadian ecozones.

167

168

169 **Methodology and Methods**

170 Core collection and shipment

171 A total of 37 sediment cores was collected from lakes across four ecozones of Eastern Canada as part of
172 the NSERC LakePulse network. Virtually all lakes greater than 0.1km² and within 1km of a road were
173 considered for selection by the modified stratified design whereby an equal number of lakes would be
174 sampled across different ecozones (CCEA Canada Ecozones V5b, 2014) as well as lake area and human
175 impact classes (Huot et al., 2019). Ecozones are defined as regional delineations of shared geological,
176 climatic and ecological characteristics (Ecological Stratification Working Group, 1996). Logistical
177 considerations meant that full cores were collected once a week, on the day before sample shipment,
178 and thus slightly altered the original stratified design. Sediment cores were retrieved using the NLA
179 Gravity corer (built by Aquatic Research Instruments) from the deepest point of the lake detected, or
180 from the deepest point of one of the lake's sedimentary basins. On the same day as core collection,
181 sodium polyacrylate was slowly added to a small volume of overlying water within the core tube to
182 stabilize the water-sediment interface for shipping (Tomkins et al., 2008). The addition was done in
183 increments (e.g., adding and waiting for stabilization) to limit porewater absorption. Once the sodium
184 polyacrylate had formed a gel, the sediment cores were stored in a cooler at 4°C until shipping (usually
185 within 24 hrs). Additional cores were also collected on the same day and extruded in the field for surface
186 and pre-industrial sediment layers (Top-Bottom), and ²¹⁰Pb activities from these secondary cores were
187 compared to the full cores. Full sediment cores were shipped on freezer packs to Laval University.
188 Shortly after arrival, these sediment cores were split longitudinally for core scanning. One of the
189 sediment core halves was kept as an archive while the other, "working half" was subsequently
190 subsampled at 1 cm intervals and placed in Whirl-pak sampling bags that were kept frozen until freeze
191 drying.

192

193 Gamma Spectroscopy

194 For each of the 37 full sediment cores, ~15 discrete sediment intervals along the depth of each core
195 were prepared for gamma spectroscopy and analyzed at the Paleoeological Environmental Assessment
196 and Research Laboratory (PEARL) at Queen's University, Canada. Briefly, sediment intervals were freeze-
197 dried, placed into gamma tubes to a height of about 2.5 cm and sealed using 2-ton epoxy over a silicone
198 septum and left to reach equilibrium for three weeks. An Ortec[®] high purity Germanium gamma
199 spectrometer (Oak Ridge, TN, USA) was then used to measure the gamma activity of the radioisotopes
200 ²¹⁰Pb, ²¹⁴Pb, ²¹⁴Bi and ¹³⁷Cs. The chronologies for these cores were derived from the measured
201 radioisotopic activity using ScienTissiME 2.1.4 software (Apr 2017) for the three dating models described
202 above.

203

204 Overview of the Three Dating Models (C.F.C.S., C.I.C., C.R.S.)

205 The *simplest* model of the three is the C.F.C.S. model. It assumes a constant sedimentation rate
206 throughout the entire sediment sequence, such that the activity of unsupported ^{210}Pb is expected to
207 decay as a function of the cumulative dry mass of sediment in a core (Crozas et al., 1964; Koide et al.,
208 1972). Dates for sediment intervals are derived graphically from the slope of the log-transformed
209 unsupported ^{210}Pb against cumulative dry mass (Sanchez-Cabeza and Ruiz-Fernandez, 2009). This dating
210 model is described as the most appropriate for lakes where erosive processes in the catchment have
211 been steady and in-lake productivity has been constant (Appleby and Oldfield, 1983), as exemplified by
212 many remote and large Alaskan lakes (Rogers et al., 2013).

213 The C.I.C. model assumes a 1st order decay of the unsupported ^{210}Pb activity. However, the C.I.C. model
214 relies on the assumption that there will be a constant activity of unsupported ^{210}Pb in each sediment
215 layer as it is formed. This model allows for variation in sedimentation rates but assumes that increases in
216 the flux of sedimentary particles from the water column will proportionally increase the ^{210}Pb deposited
217 to the sediment floor, thus yielding constant initial unsupported ^{210}Pb activities irrespective of any
218 variations in sediment accumulation rate (Appleby and Oldfield, 1983).

219 Finally, the C.R.S. model also assumes a 1st order decay rate but is based on the decay of the total
220 cumulative unsupported ^{210}Pb activity, also known as the total ^{210}Pb inventory (A_0). A_0 is the cumulative,
221 density-corrected unsupported ^{210}Pb measured across sediment intervals (Sanchez-Cabeza and Ruiz-
222 Fernandez, 2009). In this model, the underlying hypothesis is that there is a constant fallout of ^{210}Pb
223 from the atmosphere, yielding a constant rate of supply of unsupported ^{210}Pb to the sediment surface
224 (Appleby and Oldfield, 1983). However, across different layers, the unsupported ^{210}Pb of the initial
225 activity (at time zero) will be inversely proportional to the mass accumulation rate, such that increases
226 in sediment erosion or autochthonous production could result in a dilution of unsupported ^{210}Pb .

227

228

229

230

231

232

233

234

235

236

237

238 **Table 1.** Summary of dating models highlighting the key assumption and equations across each of the
 239 three main dating models. See symbols and abbreviation table.

Model	Assumption	Equations
Constant Flux Constant Sedimentation model (C.F.C.S.)	<ul style="list-style-type: none"> Assumes a constant sedimentation rate along the entire core Activity of unsupported ^{210}Pb is expected to decay as a function of the cumulative dry mass of the sediment in the core 	$\text{Log-}C_{t_x} = \text{Log-}C_0 e^{-\lambda \frac{m}{MAR}}$ $MAR_{\text{CFCS}} = \frac{-\lambda}{b}$
Constant Initial Concentration model (C.I.C.)	<ul style="list-style-type: none"> Assumes a constant activity of unsupported ^{210}Pb in each sediment layer as it is formed Increases in the flux of sedimentary particles from the water column will proportionally increase amounts of unsupported ^{210}Pb deposited to the sediment floor 	$C_{t_x} = C_0 e^{-\lambda t_x}$ $MAR_{\text{CIC}} = \frac{m_j - m_i}{\Delta t}$
Constant Rate of Supply model (C.R.S.)	<ul style="list-style-type: none"> Assumes a constant fallout of ^{210}Pb from the atmosphere, yielding a constant rate of supply of unsupported ^{210}Pb to the sediment surface Unsupported ^{210}Pb of the initial activity (at time zero) will be inversely proportional to the mass accumulation rate, such that increases in burial driven by sediment erosion or autochthonous production results in dilution of unsupported ^{210}Pb 	$A_{t_x} = A_0 e^{-\lambda t_x}$ $MAR_{\text{CRS}} = \lambda \times \frac{A_{t_x}}{C_{t_x}}$

240 Symbols used in tables: λ , ^{210}Pb disintegration constant ($\lambda = 0.03114 \text{ year}^{-1}$); m , Cumulative dry mass of
 241 sediment (g); MAR , Sediment mass accumulation rate ($\text{g cm}^{-2} \text{ year}^{-1}$); b , Slope of log-transformed C_{t_x}
 242 with cumulated dry mass ($\frac{1}{\text{g cm}^{-2}}$); C_{t_x} , Unsupported ^{210}Pb activity at time t_x (Bq kg^{-1}); t_x , Time x (year);
 243 Δt , Elapsed time between the deposition of two intervals ($\Delta t = t_i - t_j$, years); A_{t_x} , $^{210}\text{Pb}_{\text{Unsupp.}}$ accumulated
 244 below interval corresponding to time t_x (Bq m^{-2});

245

246

247 Dating Model Selection

248 To evaluate the performance of the different dating models generated by the ScienTissIME software
 249 (<http://www.scientissime.net/>), we plotted for each lake the pattern of the unsupported ^{210}Pb
 250 ($^{210}\text{Pb}_{\text{Unsupp.}}$) content measured throughout the cores as a function of the expected decaying trends
 251 across each model as detailed in Appleby and Oldfield (1983).

252

253 For the C.F.C.S. model, the log-transformed unsupported $^{210}\text{Pb}_{\text{Unsupp.}}$ was plotted against the cumulative
 254 dry mass of sediment. As described in Appleby et al. (1983), for the C.F.C.S. model to be considered
 255 valid, $\text{log-}^{210}\text{Pb}_{\text{Unsupp.}}$ must follow a linear relationship with cumulative dry mass.

256
$$\text{Log-}C_{t_x} = \text{Log-}C_0 e^{-\lambda \frac{m}{MAR}} \quad (\text{Equation 1})$$

257 Where $\log-C_{t_x}$ is the log-transformed activity of $^{210}\text{Pb}_{\text{Unsupp.}}$ (Bq kg^{-1}), $\log-C_0$ the initial log-transformed
 258 activity of $^{210}\text{Pb}_{\text{Unsupp.}}$, λ the ^{210}Pb disintegration constant ($\lambda = 0.03114 \text{ year}^{-1}$); m the cumulative dry mass
 259 of the sediment core (g) and MAR the sediment mass accumulation rate ($\text{g cm}^{-2} \text{ year}^{-1}$).

260
 261 To evaluate performance of the C.I.C. model, we modeled the expected decay of the measured
 262 $^{210}\text{Pb}_{\text{Unsupp.}}$ activity as a function of cumulative dry mass. To allow for the 1st order reaction to reach
 263 “background” activity (= where the unsupported ^{210}Pb level reaches the supported ^{210}Pb activity; ~1900
 264 CE) at the observed cumulative dry mass, we incorporated the measured cumulative dry mass where
 265 background is reached (m_{bdg}) as the denominator of the decaying-section of the equation (= exponent
 266 denominator) and replaced $\lambda * t_x$ by the ratio of age-background ($t_{\text{bgd}} = 1900 \text{ CE}$) and ^{210}Pb half-life
 267 ($t_{1/2} = 22.23 \text{ years}$).

268
 269
$$C_{t_x} = C_0 e^{-\lambda t_x} = C_0 e^{-\frac{t_{\text{bgd}}}{\frac{t_{1/2}}{2}} \cdot \text{g cm}^{-2} \text{ yr}^{-1}} \quad (\text{Equation 2})$$

270
 271
 272 The expected decay rate associated with validation of the C.R.S. models followed a similar methodology
 273 as for the C.I.C. expected decay profile, but further considered the 1st-order decay rate of the ^{210}Pb
 274 inventory, which evaluates the density-corrected cumulative content of $^{210}\text{Pb}_{\text{Unsupp.}}$: A_0 (Bq m^{-2}). Similar
 275 to what has been previously described, the ^{210}Pb inventory was modeled to decay as a function of
 276 cumulative dry mass where ^{210}Pb inventory reaches background supported ^{210}Pb .

277
 278
$$A_{t_x} = A_0 e^{-\lambda t_x} = A_0 e^{-\frac{t_{\text{bgd}}}{\frac{t_{1/2}}{2}} \cdot \text{g cm}^{-2} \text{ yr}^{-1}} \quad (\text{Equation 3})$$

279 To compare models and select the most robust among them, we evaluated the fit (R^2) between
 280 observed ^{210}Pb content and predicted ^{210}Pb quantities derived from the expected decaying trends. To
 281 remove the scale impact in relation to the different ^{210}Pb quantities evaluated ($\log-^{210}\text{Pb}_{\text{Unsupp.}}$ for
 282 C.F.C.S., $^{210}\text{Pb}_{\text{Unsupp.}}$ for C.I.C. and ^{210}Pb Inventory for C.R.S.), we Z-transformed the observed and the
 283 predicted ^{210}Pb quantities and calculated the resulting Z-scaled Root Mean Squared Error (Z-RMSE). The
 284 model returning the greatest R^2 and the lowest Z-RMSE values was then selected. A summary of the
 285 steps taken towards model selection is available in the supplementary materials (Fig S1). Chronologies
 286 from selected dating models yielding non-increasing age-depth relationships were rejected, and instead
 287 were selected chronologies from the dating model returning the second highest R^2 and second lowest Z-
 288 scaled RMSE. Lake sediment cores displaying both a uniform $^{210}\text{Pb}_{\text{Total}}$ distribution along core depth and
 289 the lack of a distinct ^{137}Cs peak should also qualify for rejection because of concerns over potential

290 mixing and/ or re-distribution of $^{210}\text{Pb}_{\text{Total}}$, thereby violating dating model assumptions. In general, a
291 thorough investigation of the resulting mass accumulation rates should be performed, leading to the
292 potential rejection of the chronology when anomalous MAR estimates have been identified.

293

294

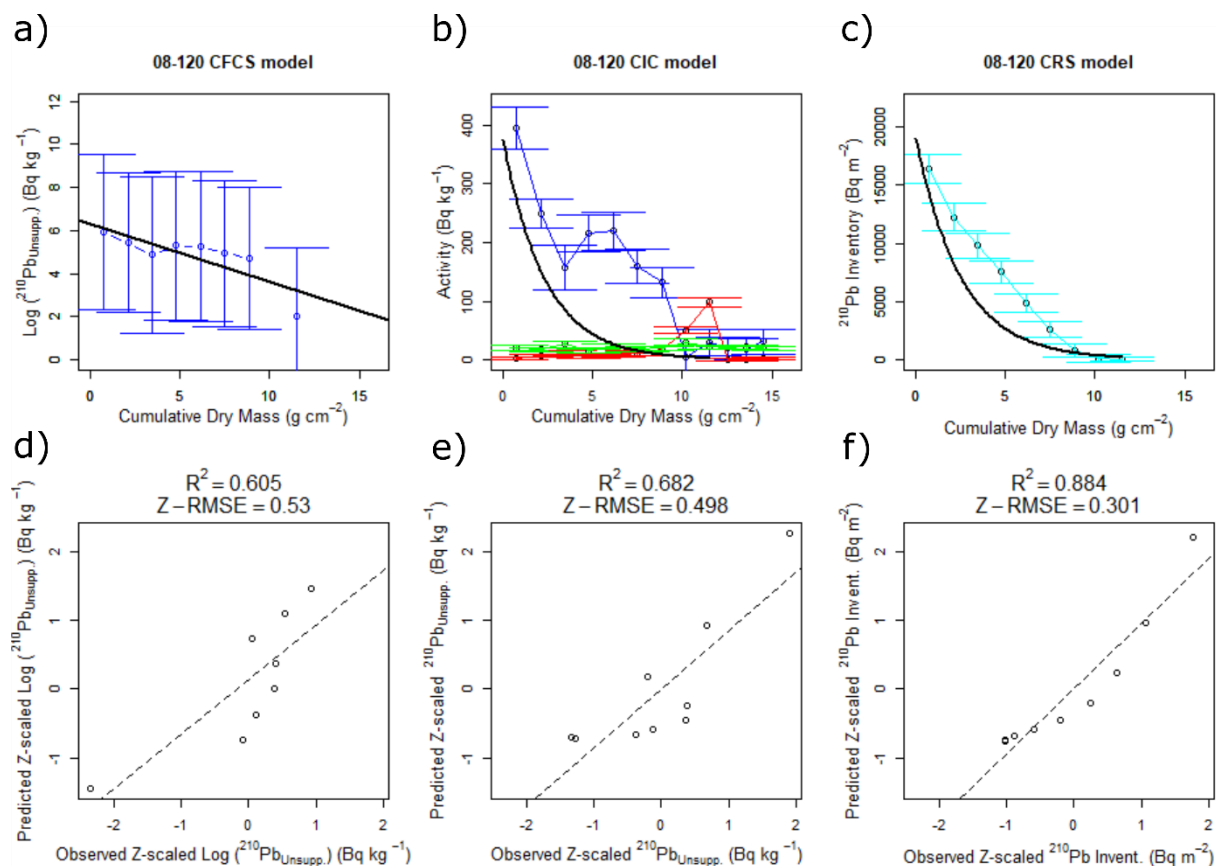
295 General errors and chronological uncertainty

296 Analytical errors linked with gamma detection of the naturally occurring radioisotopes were reported
297 following the equation provided in Sanchez-Cabeza and Ruiz-Fernandez (2012). This error was
298 propagated to the calculation of age estimates using empirical equations as it is generated in
299 ScienTissiME 2.1.4. Another error in establishing core chronologies using ^{210}Pb is if the uppermost
300 unconsolidated section is not retrieved by the coring device (Crusius and Anderson, 1991) or was
301 potentially influenced by the sodium polyacrylate addition. To evaluate these processes, we compared
302 ^{210}Pb unsupported activities from the first subsampled interval of our full sediment cores (0-1 cm) to the
303 *Top* (0-1 cm) sample collected from the additional sediment cores (Top-Bottom) retrieved the same day
304 and extruded in the field. This comparison yielded a robust correlation coefficient ($R^2 = 0.64$) indicative
305 that the ^{210}Pb activities in the top intervals of the full sediment cores were similar between cores. Due to
306 the large-scale nature of the sampling protocol the full sediment cores were sub-sectioned horizontally
307 every cm in the lab. This coarse subsampling led to a reduction in the number of intervals available for
308 dating model selection in regions of low sedimentation rates, likely reducing the robustness in model
309 selection. For each derived chronology, age estimates were compared to the natural ^{137}Cs maximum
310 abundance found within each sediment core, but with full knowledge that the ^{137}Cs peak may be mobile
311 within the sediment column (see Metadata). To compensate for the coarse subsampling resolution
312 when investigating naturally occurring ^{137}Cs maximum in sediment stratigraphies, we used a spline
313 interpolation to model the raw abundance of ^{137}Cs across sediment intervals. A graphical representation
314 of each radioisotope profile was made against the expected decay profile across each model, and the fit
315 between expected ^{210}Pb , generated from empirical equations, and observed ^{210}Pb activity measured
316 across intervals was compared by linear regression (Figure 2).

317

318

319



320
 321 Figure 2. Multi-panel plot summarizing the empirical ²¹⁰Pb dating model fitting (detailed in Appleby and
 322 Oldfield (1983), and evaluation using linear regression for lake 08-120 (Lac des Chicots – Ste Therese,
 323 QC). a) Log-transformed ²¹⁰Pb_{Unsupp.}, with error bars in blue as a function of cumulative dry mass. The
 324 black line represents the best linear model fit. b) Graphical representation of the measured ²¹⁰Pb (Bq kg⁻¹)
 325 in blue with corresponding errors as a function of cumulative dry mass. The red line is the ¹³⁷Cs
 326 activities (Bq kg⁻¹) and the ²¹⁴Bi activities are in green. The black line is the expected decay curve for
 327 ²¹⁰Pb_{Unsupp.} c) Graphical representation of the observed ²¹⁰Pb inventory and corresponding errors in cyan,
 328 as a function of cumulative dry mass. The black line is the expected decay curve for ²¹⁰Pb inventory. d)
 329 Linear regression evaluating the fit of the predicted log Z-transformed ²¹⁰Pb_{Unsupp.} activities (Bq kg⁻¹)
 330 against observed log Z-transformed ²¹⁰Pb_{Unsupp.} e) Linear regression evaluating the fit of the predicted Z-
 331 transformed ²¹⁰Pb_{Unsupp.} activities (Bq kg⁻¹) against observed Z-transformed ²¹⁰Pb_{Unsupp.} f) Linear
 332 regression evaluating the fit of the predicted Z-transformed ²¹⁰Pb inventory (Bq m⁻²) against the
 333 observed Z-transformed ²¹⁰Pb inventory. The R² of the relationship and the RMSE of the Z-transformed
 334 observed and predicted ²¹⁰Pb quantities for each of the three models appears on top of each graph from
 335 d – f.

336

337 Sediment Mass Accumulation Rate Calculation

338 Lake sediment mass accumulation rates were calculated following model-specific equations.

339 For the C.F.C.S. model, sediment Mass Accumulation Rate (MAR_{CFCS} , g cm⁻² year⁻¹) was calculated based
 340 on the slope of the natural log unsupported ²¹⁰Pb (Log-C_x) regression as a function of cumulative dry

341 mass. Following the parametric equation “ $y = a + bx$ ”, a equals log-transformed C_0 and b ($\frac{1}{g\text{ cm}^{-2}}$) is the
 342 slope of the log-transformed C_x relationship with cumulative dry mass. MAR can be derived using the
 343 following:

$$344 \quad \text{MAR}_{\text{CFCS}} = \frac{-\lambda}{b} \quad (\text{Equation 4})$$

345
 346 For the C.I.C. model, sediment mass accumulation rate (MAR_{CIC} , $\text{g cm}^{-2} \text{ year}^{-1}$) was calculated from the
 347 mass difference between two intervals i and j (m_i and m_j) and the associated elapsed time between the
 348 deposition of these two layers ($\Delta t = t_i - t_j$, years)

$$349 \quad \text{MAR}_{\text{CIC}} = \frac{m_j - m_i}{\Delta t} \quad (\text{Equation 5})$$

350
 351 For the C.R.S. model, sediment mass accumulation rate (MAR_{CRS} , $\text{kg m}^{-2} \text{ year}^{-1}$) was calculated for each
 352 interval based on the proportion of unsupported ^{210}Pb (C_{t_x} , Bq kg^{-1}) to cumulative ^{210}Pb inventory from
 353 the bottom of the core to interval corresponding to time t_x (Bq m^{-2}).

$$354 \quad \text{MAR}_{\text{CRS}} = \lambda \times \frac{A_{t_x}}{C_{t_x}} \quad (\text{Equation 6})$$

355
 356 MAR_{CRS} is obtained by means of a ratio, and low C_i values can be measured when approaching
 357 background supported ^{210}Pb activity; as a result, artificially elevated values in MAR_{CRS} can be detected.
 358 For this reason, we removed one estimate of MAR_{CRS} associated with lake 08-179 where the specific
 359 MAR_{CRS} was 87 times greater than the rest of MAR_{CRS} for this lake.

360
 361 Census Population Reconstruction

362 We delineated the hydrologically conditioned watersheds of the lakes using a 20 m flow direction raster
 363 layer acquired from the 0.75 arc second Canadian Digital Elevation Model dataset (Government of
 364 Canada, 2015). The delineation uses the union of all sub-drainage basins that reach each point along a
 365 lakeshore based on the National Hydro Network lakes polygon data (Government of Canada, 2017). We
 366 then acquired Census Subdistrict (CSD) boundary files from 1911 CE to 2016 CE (accessible from:
 367 <http://geo.scholarsportal.info/>) along with the relevant microstatistics table files that feature the total
 368 population within each CSD (accessible from: <http://odesi2.scholarsportal.info/webview/>). In an effort
 369 to normalize the geographical data and to overcome issues of the Modifiable Areal Unit Problem
 370 (MAUP) (Openshaw, 1983), we used the WordPop UN dataset to redistribute CSD population counts
 371 across each CSD. To reduce the error associated with new urban development arising during the 20th
 372 century, digitized historical topographic maps were used when available. These historical maps were
 373 acquired from national and university libraries (Scholar Geoportal for Ontario, BaNQ for Quebec and
 374 from an online repository from the University of Ottawa). These maps were produced from 1909 to
 375 1989 CE at a resolution of 1:63,360 or 1:50,000. These maps were georeferenced using the WGS84
 376 coordinates present on the map. Each “house” on the maps was accounted for by a point feature. We

377 then compared our redistributed population against the georeferenced point feature layer to ensure our
378 population estimates were adequate.

379

380

381 Temporal Temperature and Precipitation reconstruction

382 Historical (1841 CE – 2017 CE) monthly records of air temperature and precipitation were obtained from
383 Environment and Climate Change Canada using the rclimateca package (Dunnington, 2018). Only
384 stations with at least a complete year of monthly data were selected to create mean annual
385 temperature and total annual precipitation estimates for each station. Rather than assigning air
386 temperature and precipitation estimates based on the nearest station (which can be hundreds of km
387 away), estimates from stations within 75 km of the study site were spatially interpolated, forming rings
388 of raster values (estimated temperature and precipitation) around the input station. This step ensured
389 that the estimated temperatures for any site were reflective of station input data.

390

391 Lake Morphometric and Watershed Land Use, Bedrock Geology and Soil Composition

392 Basic lake morphometric information was recorded across all lakes featured in this study. Lake
393 maximum depth (m) was estimated as the maximum depth measured by the field teams during
394 sampling with aid of bathymetric maps when available. Lake surface area (km²) was obtained via
395 Canvec/HydroLakes and altitude (m a.s.l.) calculated from The Canadian Digital Elevation Model (CDEM).

396 Since the methodology developed for the LakePulse pan-Canadian sampling of lakes involved
397 the classification of lakes according to the relative proportion of natural to more intensive land uses (e.g.
398 Agriculture, Urban, Mines; see Huot et al. (2019) for details) in their watersheds, we explored the
399 influence of each of these land-use types on the variation observed in lake sediment mass accumulation
400 rates. A table summarizing data sources included in Huot et al. (2019) is available in the supplementary
401 materials of this study (Table S1). We simplified the original land use definitions found in *Annual Space-
402 Based Crop Inventory for Canada* (2016) and in *Land Use* (2010) into seven categories (NoData, Water,
403 Natural Landscape, Forestry, Urban, Agriculture, Pasture and Mines). A table summarizing the original
404 class definition and the simplified categories is also available in the electronic supplementary materials
405 (Table S2).

406 To investigate the role of watershed soil and geological composition on the variation observed
407 in mass accumulation rates, we acquired bedrock geology from the Geological Survey of Canada (1996)
408 and computed the intersection between the watershed polygons and the bedrock geology polygons.
409 With one of the lakes' watersheds spanning outside of Canada into the USA, "NoData" has been
410 assigned for this portion of the watershed. Soil properties maps generated by the International Soil
411 Reference and Information Centre (ISRIC) were retrieved from *soilgrids.org*. From the available soil
412 horizon depths, we selected the 0-5m depth layer and computed for each watershed the mean
413 abundance of all soil property values.

414

415 Statistical analyses

416 All statistical modelling was performed using R (R Core Team, 2013) and all occurrences of log-
417 transformed variables refer to the common (i.e., base 10) logarithms. Specific packages used include
418 *davies.test::segmented* for the analysis of breakpoints in the regression parameter in the linear predictor
419 (Muggeo, 2003). General additive mixed effects models (GAMMs) were fitted using the R package *mgcv*
420 (Wood, 2012). A random factor was assigned to lake identity (LakeID) to structure errors in the model's
421 residuals. In GAMMs, the estimated degree of freedom (e.d.f.) summarizes the degree of non-linearity
422 of the modelled trends, with values of 1 being linear and with any value above 1 reflecting a departure
423 from linearity. To establish the potential significant differences in lake sediment mass accumulation
424 across different timesteps instructed from Davies' test, we first assessed the normality in the paired
425 MAR differences (pre and post breakpoint) for each of the four ecozones using a Shapiro-Wilk test. Since
426 all ecozone specific Shapiro-Wilk tests returned p-values greater than $p = 0.05$, the paired MAR
427 differences were considered to be normally distributed and the significant difference in means was
428 evaluated using a paired t-test. To establish a predictive model of recent mean lake mass accumulation
429 rates, we selected and averaged MAR estimates ranging from 2000 to 2017 (the latter indicative of the
430 year when the cores were retrieved). Using a post-2000 period was mainly motivated by the limited
431 availability of environmental datasets that are necessary to explore the drivers of recent lake MARs.
432 Lake specific recent mean MARs were then used in a multiple linear regression model. For this predictive
433 model, the explanatory variables that were considered included climatic variables (mean annual air
434 temperature (MAT, °C) and total annual precipitation (mm)), watershed land-use variables (fraction of
435 agriculture in the catchment (%), population count (individuals), soil and bedrock geology fractions (%)),
436 watershed size (km²), and lake morphological variables (lake depth (m), lake surface area (km²)).

437

438 **Results**

439 Assessing the Performance of Dating Models

440 Across the 37 sediment cores considered, the C.R.S. model returned higher R^2 values for 30 lakes when
441 assessing the fit between observed and predicted values of unsupported ²¹⁰Pb. The C.I.C. model typically
442 had the lowest fit, while the C.F.C.S. equation performed well in only a handful of lakes (Table 2).
443 Considering each of the four ecozones separately, the C.R.S. model always returned the highest R^2 for
444 lakes in the Mixedwood Plains region. In contrast, the C.F.C.S. model was selected as having the best fit
445 in several Boreal Shield sites, although the C.R.S. was still deemed appropriate for most lakes in this
446 ecozone. Lakes set in the two Atlantic ecozones (Atlantic Highlands and Atlantic Maritime) also
447 predominantly followed the C.R.S. exponential decay of ²¹⁰Pb inventory quantities (Table 2). While the
448 C.R.S. model generally produced a higher R^2 than the other models, for some lakes the C.F.C.S. model
449 and the C.R.S. model generated similar R^2 values (Table 3, Figure S2). Lakes with higher proportions of
450 urban land cover in their watersheds tended to display a greater R^2 difference between C.F.C.S. and
451 C.R.S. models. While the agriculture fraction within watersheds was also tested, it was not a significant
452 predictor of this difference. There was no clear spatial distribution signal in the selected chronological
453 model (Figure 3).

454

455 Table 2. Distribution of the selected dating model percentage across the four Eastern Canadian
 456 ecozones. Lakes sample size across ecozone is indicated between parentheses.

Ecozone	C.F.C.S.	C.I.C.	C.R.S.
Atlantic Highlands (11)	9%	9%*	82%
Atlantic Maritime (7)	14%	0%	86%
Boreal Shield (10)	30%	0%	70%
Mixedwood Plains (8)	0%	0%	100%

457 *Despite the C.I.C. model being selected for one of the lakes (17-067) in the Atlantic Highlands, dates for
 458 this core could not be derived using the C.I.C. equation as it generated non-decreasing age with depth
 459 (see metadata). For core 17-067, we thus generated dates using the C.R.S. model which returned similar
 460 R² to that of the C.I.C. model (see Figure S2).

461

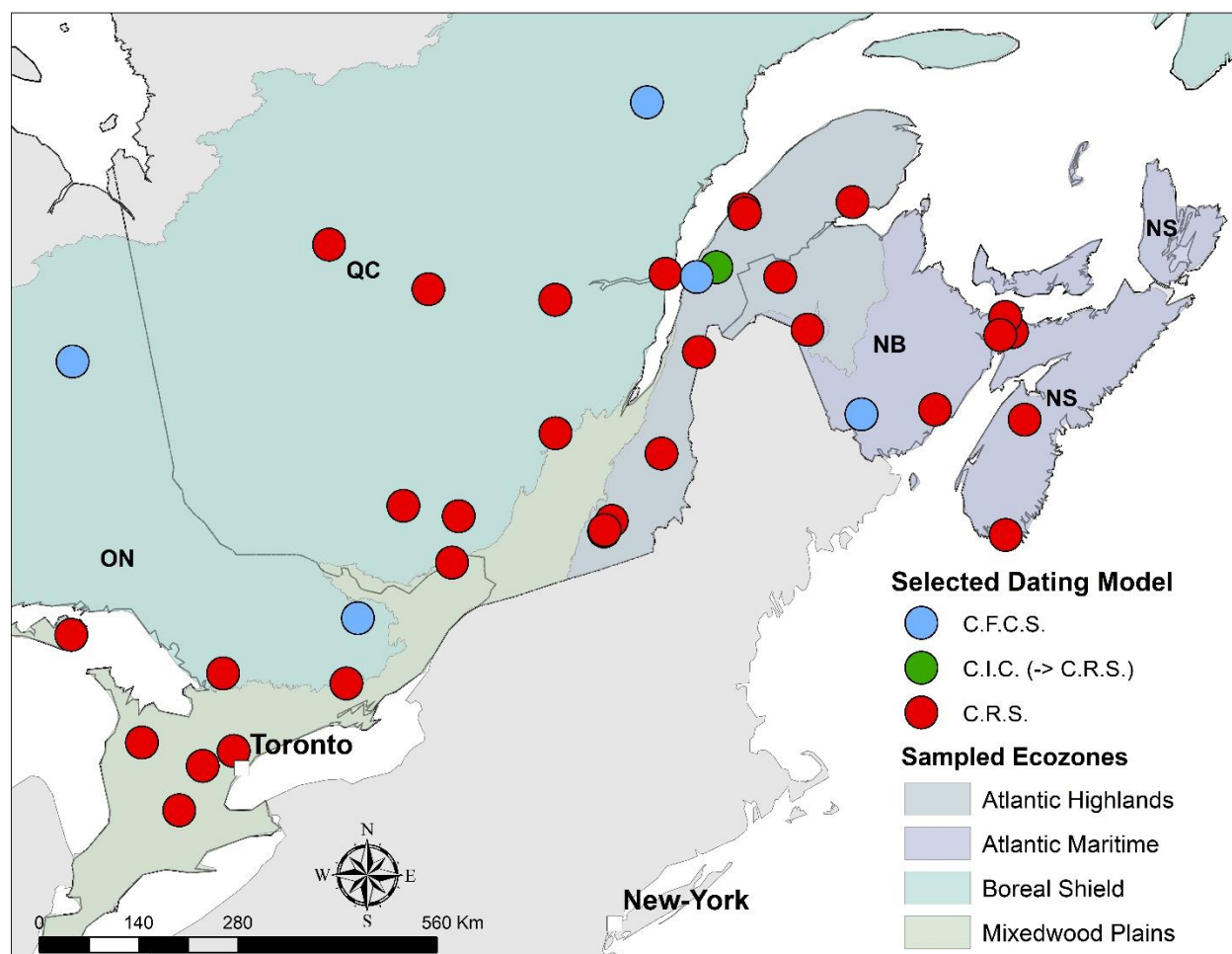
462

463

464 Table 3. Summary of the linear model R² for the three dating models tested (n=111). The *Estimate*
 465 parameter accounts for the mean R² value obtained across all 37 lakes.

Dating Model	Mean R ²	Standard Error of R ²	p-value
C.F.C.S.	0.788	0.035	< 0.001
C.I.C.	0.667	0.039	0.002
C.R.S.	0.944	0.039	< 0.001

466



467

468

469

Figure 3. Map showing the distribution of the selected dating models across the four sampled Eastern Canadian ecozones.

470

471

472

473

474 Temporal variation in sediment mass accumulation rates

475

476

477

478

479

480

481

482

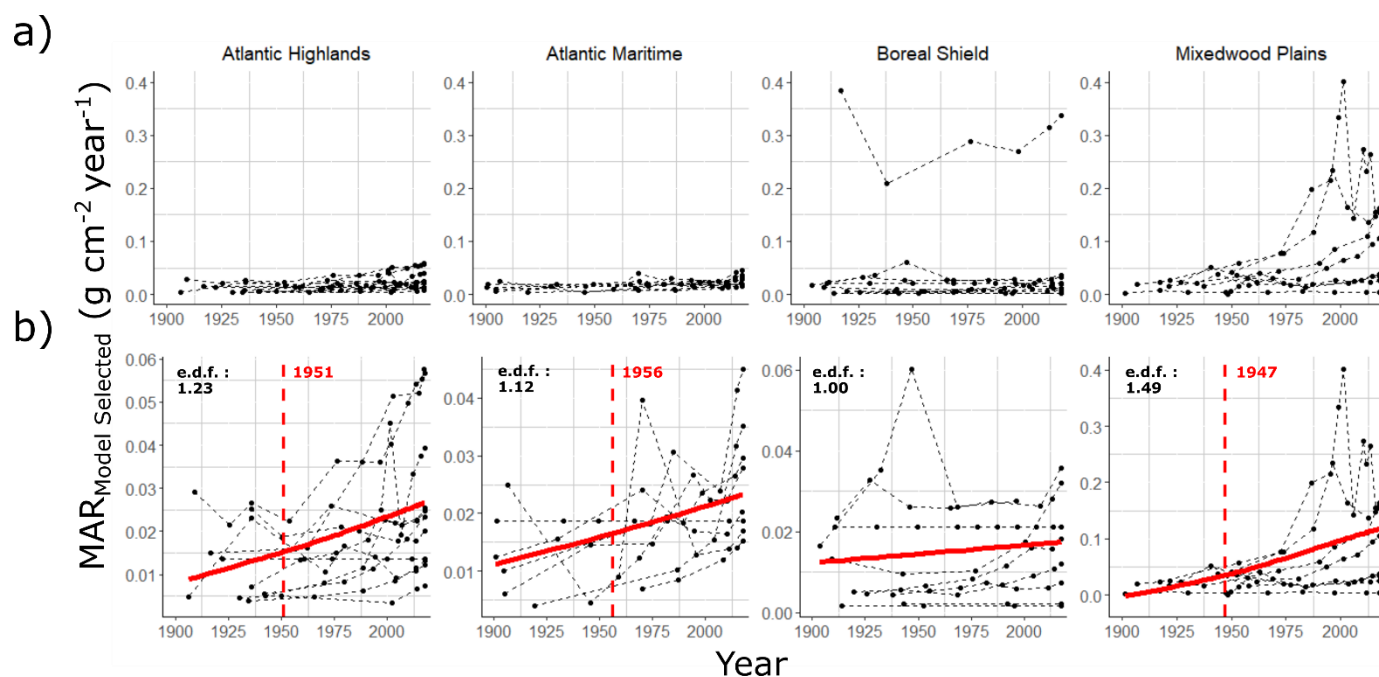
483

Using the selected dating model identified for each ecozone, we considered region-specific change in lake MARs. While pre-industrial (pre-1900) lake sediment MARs exhibited similar values across all four ecozones, with estimates ranging from 6.3×10^{-3} to $1.5 \times 10^{-2} \text{ g cm}^{-2} \text{ year}^{-1}$, there was a marked difference across ecozones, with lakes in the Mixedwood Plains (M.P.) accumulating a greater amount of sediment than lakes in the other 3 ecozones (Figure 4a). One lake set in the Boreal Shield (B.S.) had highly elevated MAR estimates compared to other lakes in this ecozone. This site is located in the floodplain of Lac St-Jean (QC), and the ^{210}Pb profile suggested numerous rapid-deposit events (see Metadata). Given that this lake (Lac à la Croix, 06-103) was not representative of its region's sedimentation rate patterns, it was removed from the dataset for any further analysis. Region-specific

484 modelled trends provided evidence of non-linear variation in MARs across three of the four ecozones
 485 evaluated, with GAM-estimated degree of freedom (e.d.f.) values ranging from 1.12 - 1.49 (Figure 4b).
 486 The Atlantic Maritime (A.M.) and Atlantic Highlands (A.H.) as well as the Mixedwood Plains displayed
 487 nearly constant rates of sedimentation prior to the 1940s. Between 1947 and 1956, rates of
 488 sedimentation accelerated across these three ecozones (supported by the Davies test results, Figure 4b).
 489 In the case of the Boreal Shield, the GAM did not detect any support for nonlinear temporal variation of
 490 MAR.

491

492



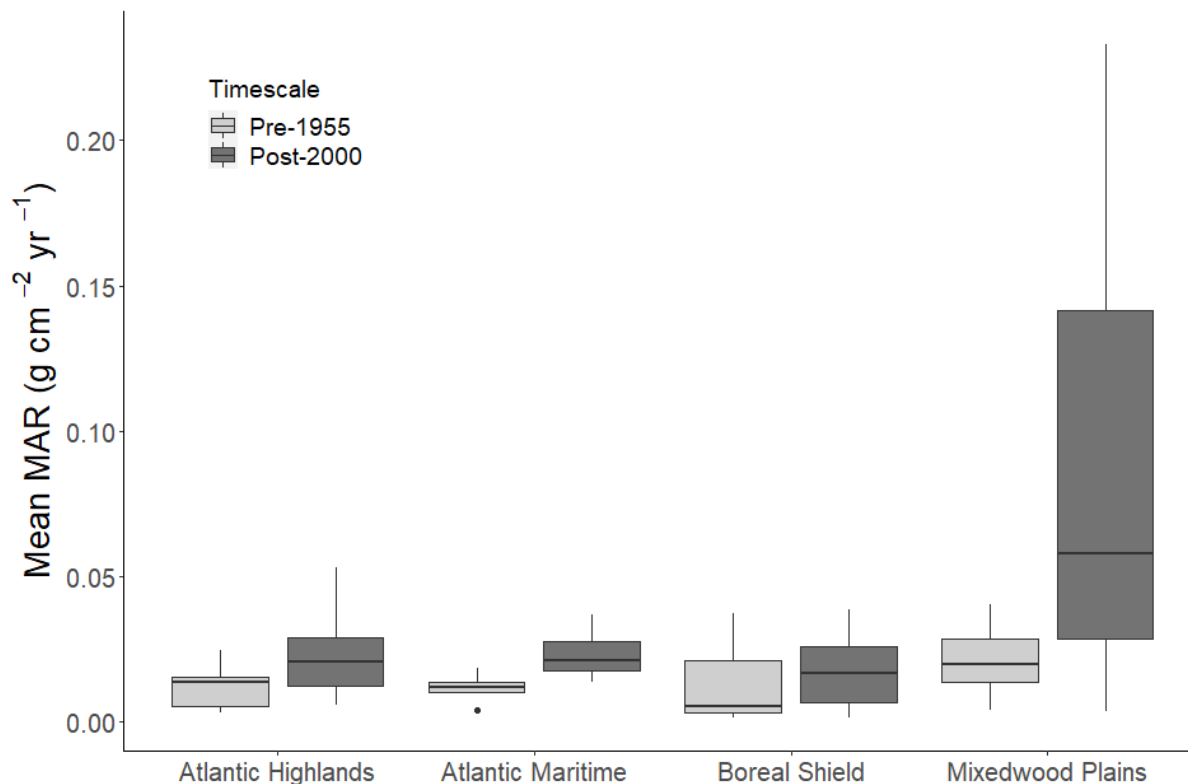
493

494 **Figure 4.** Temporal variation in sediment dry weight mass accumulation rate across the four ecozones of
 495 Eastern Canada as determined from dating model selection. a) The upper panels display the raw
 496 measured sedimentation rates across the 37 lakes. b) The lower panels show the general additive model
 497 (GAMM) trends of ecozone-specific MAR temporal variation. The estimated degrees of freedom (e.d.f.)
 498 associated with the GAMM is also reported, as is the estimated onset of the MAR acceleration across
 499 each ecozone based on a breakpoint analysis. Note: One lake (06-103) for the Boreal Shield was
 500 identified as having anomalously high MAR and was also found to be a site in a floodplain, and was thus
 501 removed from GAMM analyses.

502

503 Considering the continuous temporal variation observed for MAR and the marked acceleration
 504 in lake MAR as evidenced from the Davies test (Figure 4a and b), we considered a former timestep
 505 defined as *pre-1955 CE*, which includes MAR estimates prior to the acceleration recorded across Eastern
 506 Canada. A second timestep – *post-2000 CE*, reflective of the last ~20 years of MAR – was also considered
 507 as it is the focus of a subsequent analysis in this study where we evaluate the predictors of recent lake
 508 MARs. As described previously, using a post-2000 timestep was partly motivated by the limited

509 availability of environmental datasets which are necessary to explore the drivers of recent lake MARs.
 510 Shapiro-Wilks tests of normality demonstrated the normal distribution of the paired MAR differences in
 511 all four ecozones. Paired t-tests for each of the four ecozones evidenced significant differences in lake
 512 sediment mass accumulation rates (Figure 5). For both the Atlantic Highlands and Maritimes regions,
 513 mean MAR between time steps doubled: A.H. $t(10) = -3.17$, $p = 1.0 \times 10^{-3}$; A.M. $t(5) = -3.30$, $p = 2.1 \times 10^{-2}$.
 514 For the Mixedwood Plains, mean MAR quadrupled: $t(7) = -2.42$, $p = 4.6 \times 10^{-2}$. In contrast, the change in
 515 mean MAR across the two time periods in the Boreal Shield was more modest, but paired t-tests still
 516 detected a significant difference in lake MARs across the two timesteps considered (B.S. $t(8) = -2.72$, $p =$
 517 2.6×10^{-2}).



518 **Figure 5.** Mean Mass Accumulation Rate (MAR: $\text{g cm}^{-2} \text{ year}^{-1}$) across the four sampled Eastern Canadian
 519 ecozones for two timesteps: “Pre-1955” ($n_{\text{MARPre-1955}} = 34$), “and “Post-2000” ($n_{\text{MARPost-2000}} = 36$). While
 520 pre-1955 includes MAR estimates prior to the acceleration recorded across Eastern Canada, we also
 521 considered a post-2000 timestep, reflective of the recent MAR estimates. This timestep was considered
 522 as it is the focus of a predictive model assessing the drivers of recent lake MARs. Using this former
 523 timestep was also motivated by the limited availability of contemporary environmental datasets which
 524 are necessary to explore the drivers of recent lake MARs.
 525

526

527

528 Temporal drivers responsible for increased lake sediment mass accumulation rates

529 We applied a linear mixed effects model, correlating our estimates of mass accumulation rates year by
 530 year with population counts (number of individuals; measured approximately every 5 years), climate
 531 estimates (Mean Annual air Temperature (MAT, °C) and total annual precipitation (mm)) linearly
 532 approximated to the same year as the MAR estimate, to evaluate the temporal drivers of variation and
 533 the spatial component of the dataset as accounted for by using lakeID as a random effect. We found
 534 that mass accumulation rates (log-transformed) were positively related to log(x+1) transformed
 535 population count in the watershed (Slope = 0.177 (± 0.046), D.F. = 146, p-value = < 0.001). MAT (°C) was
 536 also found to be positively related to log-transformed lake MAR, but its contribution to the model was
 537 smaller than that of population count (Slope = 0.0912 (± 0.046), D.F. = 146, p-value = 0.0515). Overall,
 538 our regression model, which considered ~120 years of sedimentation rates for 37 sediment cores, was
 539 capable of accounting for 22% of the variation in its fixed effects. We also tested mean total annual
 540 precipitation (derived from Environment and Climate Change Canada monitoring stations) as a predictor
 541 for temporal variation in MAR, but it was not a significant parameter in the linear mixed effects model.
 542 However, LakeID as a random factor explained a large proportion (49%) of the residual variation (Table
 543 4).

544

545

546 Table 4. Summary of the linear mixed effects model assessing the temporal variation in log-transformed
 547 Mass Accumulation Rate (MAR) across the 37 cores. t-value refers to the t statistics. LLR refers to the
 548 log-likelihood ratio.

Effect	Estimate (Std. Error)	Degree of Freedom	t-value	LLR	p-value
(Marginal R² = 0.222, Conditional R² = 0.696)					
Intercept	-5.29 (0.30)	146	-17.52		
Log-(Population+1) (numbers of individuals)	0.177 (0.046)	146	3.84	17.17	0.0002
MAT (°C)	0.0912 (0.046)	146	1.96	3.85	0.0515
Random effects (Proportion of variance explained by LakeID = 0.710)					
LakeID	0.714 (0.51)			116.12	< .001
Residual	0.571 (0.32)				

549

550

551

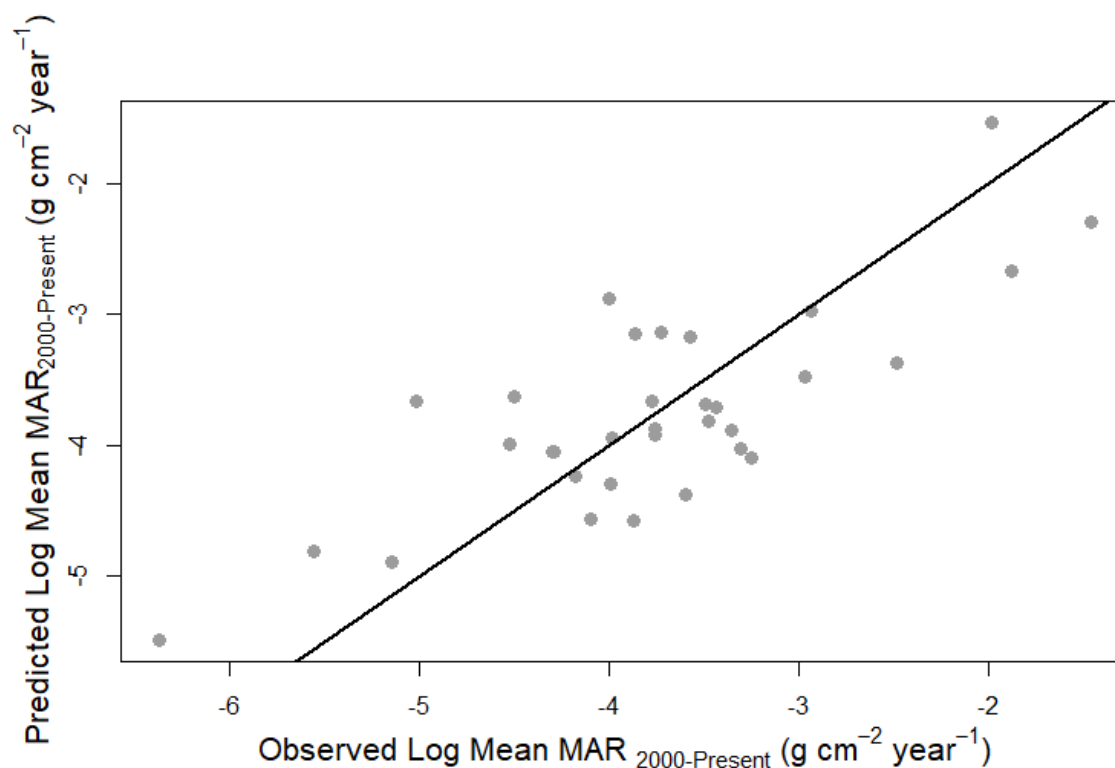
552 Predictive model for recent lake sediment average mass accumulation rates

553 Through multiple linear regression, we investigated the cross-lake variation in modern mean MAR post-
 554 2000 CE (all MAR estimates from a single lake averaged between 2000 – 2017 and expressed MAR_{2000-}
 555 $_{Present}$, $g\ cm^{-2}\ year^{-1}$) to identify significant predictors of this variation. Anthropogenic indicators,
 556 specifically the fraction of agriculture expressed in percent (p -value = 2.5×10^{-4}) and log-transformed
 557 human population count (number of individuals) (p -value = 1.1×10^{-4}) in lakes' watersheds averaged
 558 between 2000 and 2016 explained the greatest amount of variation in recent lake sediment mass
 559 accumulation rates. Another variable that accounted for a significant portion of the variation was mean
 560 total annual precipitation (over the post-2000 CE period; p -value = 2.4×10^{-4}). Altogether these variables
 561 accounted for 57% of the variation observed in average recent lake sediment mass accumulation rates
 562 (post-2000 CE) (Figure 6). Additional variables, such as the proportion of sand in the lake watershed and
 563 log-transformed lake maximum depth, were also found to be weakly significant (p -value < 0.1) but were
 564 omitted from the regression equation to prevent over-fitting of the model. The final model is expressed
 565 as:

566 $Log(Mean\ MAR_{2000-Present})\ (g\ cm^{-2}\ year^{-1}) = -8.86 + 4.3 \times Mean\ Agriculture_{2000-Present}\ (\%) + 0.22 \times$
 567 $Log(Population\ Count_{2000-Present} + 1)\ (individuals) + 0.0036 \times Mean\ Precipitation_{2000-Present}\ (mm)$

568 (Equation 6)

569



570

571 **Figure 6.** Observed versus predicted log-transformed Mean Mass Accumulation Rate (post-2000 CE,
572 from equation 6).

573

574 **Discussion**

575 Developing a robust chronology and calculating mass sediment accumulation data are critical steps in
576 most paleolimnological and biogeochemical lake studies. The new insights gained from our inter-
577 regional study of lake core dating and sedimentation rates are methodological and data-driven. On the
578 methodological front, we present a robust empirical framework for evaluating the three most
579 commonly used chronological dating models. Applying this new framework whereby we fit model-
580 specific empirical equations and compared the outcomes statistically to 37 sediment core records from
581 across 4 ecozones, we clearly showed substantial spatio-temporal variation, for which we identified
582 significant predictors.

583 Earlier work had shown that the C.R.S. model dating results are those most frequently reported in the
584 literature, but it is not always clear why this approach was adopted. The difficulty of dating model
585 selection becomes even greater when the number of sediment cores to be dated increases, or with
586 growing spatial coverage. However, this challenge can now be met with the approach we have described
587 for assessing how closely the measured isotopic activities are in accordance with the specific
588 assumptions of the chronological model. This standardized method of evaluating different chronologies
589 will further facilitate identification of the most reliable chronological dating model where model
590 assumptions are respected. Interestingly, Barsanti et al. (2020) recently conducted an interlaboratory
591 calibration exercise with 14 different laboratories worldwide to evaluate a single lake sediment isotopic
592 profile and no consensus was reached with regard to dating model selection: seven laboratories
593 selected the C.R.S. model, five adopted the C.F.C.S. model, another one chose the C.I.C model, and
594 finally the last group selected a modified version of the C.F.C.S. model. Clearly, there is a need to
595 standardize approaches to model selection.

596 From a mathematical perspective, there is a greater probability of obtaining a better R^2 value when
597 considering the C.R.S. or the C.F.C.S. model assumption over the C.I.C. model. Specifically, the C.F.C.S.
598 model is based on analyses of log-transformed ^{210}Pb activity, which reduces to some extent the
599 stochastic nature of radioisotopic measurements in sediment and thus one can expect a stronger fit
600 relative to C.I.C. model results. For the C.R.S. model, the analyses are based on the cumulative ^{210}Pb
601 inventories and it is thus less sensitive to inter-sample variation that could be apparent with C.I.C.
602 models. Independent of the dating model, the establishment of a robust chronology also depends on
603 the number of sediment intervals with measurable $^{210}\text{Pb}_{\text{unSUPP}}$ exceeding equilibrium with $^{210}\text{Pb}_{\text{SUPP}}$. For
604 this reason, it is recommended to adjust sediment core subsampling according to empirical regional
605 sedimentation rates.

606 The selection of chronological dating models across the 37 sediment cores using our framework was in
607 line with findings from the literature, where the C.R.S. model was selected the most frequently (Dillon et
608 al., 1986; Appleby, 2002). Our observation that the C.R.S. model was the most appropriate for 100% of
609 lakes studied from the Mixedwood Plains suggests that changes in sedimentation rate are common in
610 this region, which is a plausible hypothesis as this ecozone is the most densely populated region of
611 Canada. In the Atlantic Highlands and Atlantic Maritimes, a majority of cores (> 80%) displayed ^{210}Pb

612 activities best modeled following the C.R.S. model assumptions *and* showed increased sedimentation
613 rates. Increased sedimentation rates were not unexpected, either, given the long history of settlement
614 in the area. By contrast, 30% of the cores from the Boreal Shield had ^{210}Pb activities that matched most
615 strongly with the C.F.C.S. model's assumption (i.e., a consistent a log-linear decay of ^{210}Pb activities with
616 cumulative dry mass). The C.F.C.S. model was designed for lakes where erosive processes in the
617 catchment are steady and in-lake productivity is constant (Appleby and Oldfield, 1983), which aligns
618 with the more pristine and remote lakes settings of many lake-watershed ecosystems in the Boreal
619 Shield. It is also interesting that while only one of the 37 sediment cores followed the C.I.C. model's
620 assumptions, dates generated by this model could not be applied due to non-decreasing age with depth.
621 While Appleby and Oldfield (1992) described an example where the chronological C.R.S. model was
622 invalidated due to discontinuity within the sediment stratigraphy, the lake in our study for which C.I.C.
623 was selected was not one exhibiting the most drastic stratigraphic changes. We thus recommend a
624 careful contextualization of stratigraphical facies with radioisotope profiles (^{210}Pb , ^{137}Cs and ^{241}Am).

625 One of the challenges with developing an empirical means to estimate chronologies from ^{210}Pb is the
626 establishment of the expected ^{210}Pb decay trend. We must assume the age associated with the sediment
627 cumulative dry mass where unsupported ^{210}Pb activity has reached supported ^{210}Pb activity ($= t_{bgd}$) (see
628 Equations 2- 3). Depending on lake location, one can often detect 4-5 half-lives before reaching the
629 supported ^{210}Pb activity. However, at high latitudes, where the flux of atmospheric ^{210}Pb can be lower
630 (Baskaran and Naidu, 1995; Tomkins et al. 2009) or at locations where elevated autochthonous
631 production leads to the dilution of unsupported ^{210}Pb in the sediment (Binford and Brenner, 1986; Arias-
632 Ortiz et al., 2018), the number of half-lives detected can decrease on the order of 1-3 half-lives. In our
633 study, the estimated age of background was selected to be 110 years, which corresponds to 5 half-lives.
634 Results of the sensitivity analysis (Fig S3) demonstrated that the model selection we present in this
635 manuscript was consistent across the range of naturally expected values for t_{bgd} (80 – 130 years) and
636 did not elicit any analytical artifacts as can be seen outside of this range.

637 While we have highlighted the models with the best fit, it should be noted that in many cases
638 the R^2 values were very close across dating models for the same core (Fig S2). In such cases there was an
639 important overlap between dating models, at least for the uppermost section of the cores (see
640 Metadata) prior to C.R.S. model yielding older age estimates for bottom samples. While this
641 phenomenon has been described elsewhere (Turner et al., 1995; Bruel and Sabatier, 2020), our results
642 further reinforce the need to cautiously consider these older dates and evaluate different dating
643 models. With only a few lakes not returning C.R.S. as the best dating model, we did not observe striking
644 regional differences when using MAR estimates derived solely from the C.R.S. models (Figure S4).

645 Mass accumulation rates across ecozones generally matched previous estimates from the
646 literature and varied substantially across lakes within regions and also across ecozones. Set in similar
647 geological environments rich in granite and gneiss, with cool and moist climates, the Atlantic Highlands
648 and Atlantic Maritimes had similar MAR estimates. Greater proportions of sand in these lakes'
649 watersheds were found to negatively influence MAR, and the contemporary anthropogenic
650 development experienced predominantly in the coastal lowland areas of these regions could be at play.
651 The lakes from the Boreal Shield are in a different geological and hydrological region defined by a strong
652 continental climate and Precambrian granitic bedrock and, surprisingly, were not characterized by lower
653 mean mass accumulation rates. Lakes from the Boreal Shield also experienced less development of
654 anthropogenic land use within their watersheds (Huot et al., 2019). In contrast, lakes from the

655 Mixedwood Plains which are associated with a warmer climate and lie in watersheds with fertile soils,
656 along with more extensive anthropogenic development, accumulated a significantly greater mass of
657 sediment than the three other ecozones. When breaking down the temporal variation into two
658 timeframes (pre-1955 and post-2000 CE), it is apparent that all 37 lakes accumulated comparable
659 amounts of sediment prior to the 20th century. With all four ecozones having similar baseline mass
660 accumulation rates, ranging from $\sim 6.3 \times 10^{-3}$ to $1.5 \times 10^{-2} \text{ g cm}^{-2} \text{ year}^{-1}$, it is lakes from the Mixedwood
661 Plains that have recorded the largest increases in sediment MAR.

662 From the ecozone-specific General Additive Models, we can conclude that MAR estimates in the Boreal
663 Shield exhibited a linear temporal increase while the other 3 ecozones displayed non-linear temporal
664 variation in MARs with GAM e.d.f. values ranging from 1.12 to 1.49. Another commonality found across
665 these three ecozones was the timing of the MAR acceleration onset. Lakes in the Mixedwood Plains and
666 Atlantic Highlands ecozones were first to experience MAR acceleration with estimated onset occurring
667 around 1947 and 1949, respectively. Lakes in the Atlantic Highlands closely followed with a recorded
668 MAR onset around 1958. These reported onset MAR values are similar to those identified from global
669 lake sediment assessments. For example, in Baud et al. (2021), an onset of global MAR acceleration was
670 identified around 1941 and was explained by widespread increases in anthropogenic landscape
671 transformations and application of fertilizer. Echoing these findings, our results from the linear mixed
672 effects model detected significant associations between sediment MAR and anthropogenic land-use
673 variables, where percent agriculture and population count in lake watersheds were found to be
674 significant predictors. While climate accounted for some variation in sediment mass accumulation rates
675 when evaluating recent average MAR, it did not account for a significant part of the variation when
676 assessing the temporal variation in MAR. The lack of historical climate data that are distributed in
677 sufficiently close proximity to our sites in Eastern Canada may be part of the problem. Indeed, only a
678 few stations in the Boreal Shield region were available, limiting the scope of the analysis. When
679 considering additional variables, such as the geological characteristics of the watershed or lake
680 morphometric variables (lake area, lake maximum depth), the fraction of sand present in the lake
681 watershed and log-transformed lake maximum depth were only marginally significant (p -value < 0.1).

682

683 **Conclusion**

684 We generated a framework to examine ^{210}Pb activities to enable dating model selection following a
685 repeatable and quantifiable approach. Using this approach, the C.R.S. dating model was selected as the
686 most robust model for a majority of sites. We identified heterogeneity across ecozones of eastern
687 Canada in terms of the amount of sediment that lakes accumulate. Mixedwood Plains lakes accumulated
688 on average 4 times more sediment than any of the three other ecozones. While all four ecozones of
689 Eastern Canada have recorded temporal increases in lake sediment MAR since 1880 CE, it is the
690 Mixedwood Plains ecozone that recorded the greatest increase with over a 4-fold increase from baseline
691 rates. We conclude that the likely influence of population size in the watershed and increasing
692 temperatures were significant predictors for this MAR temporal variation. We also found that current
693 mean lake sediment MAR can be predicted using anthropogenic land-use variables (population count
694 and percent agriculture) along with precipitation within the watershed. Bridging the analytical model
695 selection and the derived implication for lake sedimentation provides a comprehensive approach for

696 dealing with sedimentation rate variations, which in turn is critical for the establishment of mass-
697 balance models evaluating sediment constituents such as carbon and heavy metals.

698

699 **Acknowledgements**

700 This work has been supported by a FRQNT Fellowship and an Excellence award from the Department of
701 Biology at McGill University awarded to AB. In addition, we acknowledge funding from an FRQNT Team
702 grant awarded to IGE, DA, PdG and PF, the NSERC LakePulse network as well as CRC grants awarded to
703 IGE, DA and PF. We'd also like to thank Yohanna Klanten and Julie Nadeau for subsampling the 2017
704 LakePulse cores, Michelle Gros for processing the core samples and Chris Grooms for running the
705 gamma spectroscopy.

706

707 **Author Contributions**

708 AB & IGE designed the study. IGE, PF, DA, PdG, JS & YH are responsible for funding acquisition. AB
709 responsible for methodological development. AB, MF & CA were involved in data collection. AB, CA &
710 HG participated in data investigation. All participating authors were also involved in reviewing and
711 editing of the manuscript.

712

713

714

715

716

717

718

719

720

721

722

723

724

725

726

727 **References**

- 728 Appleby, P. G. and Oldfield, F. (1978). The calculation of lead-210 dates assuming a constant rate of
729 supply of unsupported 210Pb to the sediment. *Catena*, 5(1), 1-8.
- 730 Appleby, P. (2002). Chronostratigraphic techniques in recent sediments. In: Last, W. and Smol, J.P.
731 Editors. Tracking environmental change using lake sediments: Vol 1. Basin analysis, coring, and
732 chronological techniques. (pp. 171-203) *Springer*.
- 733 Appleby, P. and Oldfield, F. (1983). The assessment of ²¹⁰Pb data from sites with varying sediment
734 accumulation rates. *Hydrobiologia*, 103(1), 29-35.
- 735 Appleby, P., Richardson, N. and Nolan, P. (1991). ²⁴¹Am dating of lake sediments. *Hydrobiologia*, 214(1),
736 35-42.
- 737 Arias-Ortiz, A., Masqué, P., Garcia-Orellana, J., Serrano, O., Mazarrasa, I., Marbà, N., Lovelock, C.E.,
738 Lavery, P.S. and Duarte, C.M., (2018). Reviews and syntheses: ²¹⁰Pb-derived sediment and carbon
739 accumulation rates in vegetated coastal ecosystems—setting the record straight. *Biogeosciences*, 15(22),
740 6791-6818.
- 741 Barsanti, M., Garcia-Tenorio, R., Schirone, A., Rozmaric, M., Ruiz-Fernández, A.C., Sanchez-Cabeza, J.A.,
742 Delbono, I., Conte, F., Godoy, J.D.O., Heijnis, H. and Eriksson, M., (2020). Challenges and limitations of
743 the ²¹⁰Pb sediment dating method: Results from an IAEA modelling interlaboratory comparison exercise.
744 *Quaternary Geochronology*, 59, 101093.
- 745 Baskaran, M. and Naidu, A. (1995). ²¹⁰Pb-derived chronology and the fluxes of ²¹⁰Pb and ¹³⁷Cs isotopes
746 into continental shelf sediments, east Chukchi Sea, Alaskan Arctic. *Geochimica Et Cosmochimica Acta*,
747 59(21), 4435-4448.
- 748 Baud A., Jenny J.P., Francus P. and Gregory-Eaves I. (2021) Global spatio-temporal analyses identify an
749 acceleration of lake sedimentation rates associated with modern land-use change. *Journal of*
750 *Paleolimnology*.
- 751 Binford, M. W. and Brenner, M. (1986). Dilution of ²¹⁰Pb by organic sedimentation in lakes of different
752 trophic states, and application to studies of sediment-water interactions. *Limnology and Oceanography*,
753 31(3), 584-595.
- 754 Binford, M. W., Kahl, J. S. and Norton, S. A. (1993). Interpretation of ²¹⁰Pb profiles and verification of the
755 CRS dating model in PIRLA project lake sediment cores. *Journal of Paleolimnology*, 9(3), 275-296.
- 756 Blais, J. M., Kalff, J., Cornett, R. J. and Evans, R. D. (1995). Evaluation of ²¹⁰Pb dating in lake sediments
757 using stable Pb, ambrosia pollen, and ¹³⁷Cs. *Journal of Paleolimnology*, 13(2), 169-178.
- 758 Bruel, R. and Sabatier, P. (2020). Serac: A package for ShortlivEd RAdionuclide chronology of recent
759 sediment cores. *Journal of Environmental Radioactivity*, 225, 106449.
- 760 Canadian Council on Ecological Areas (2014) Canada Ecozones. Version 5b [shapefile].

- 761 Center for Agroclimate, Geomatics and Earth Observation, Science and Technology Branch, Agriculture
 762 and Agri-Food Canada. Annual space-based crop inventory for Canada, Albers conic equal area, 30m
 763 [GeoTIFF].
- 764 Center for Mapping and Earth Observation, Natural Resources Canada. (2017). CanVec manmade
 765 features, NAD83 CSRS, 50k [shapefile].
- 766 Center for Mapping and Earth Observation, Natural Resources Canada. CanVec resource management
 767 features, NAD83 CSRS, 50k [shapefile].
- 768 Crozaz, G., Picciotto, E. and De Breuck, W. (1964). Antarctic snow chronology with Pb²¹⁰. *Journal of*
 769 *Geophysical Research*, 69(12), 2597-2604.
- 770 Crusius, J. and Anderson, R. F. (1991). Core compression and surficial sediment loss of lake sediments of
 771 high porosity caused by gravity coring. *Limnology and Oceanography*, 36(5), 1021-1030.
- 772 Davis, R. B., Hess, C. T., Norton, S. A., Hanson, D. W., Hoagland, K. D. and Anderson, D. S. (1984). ¹³⁷Cs
 773 and ²¹⁰Pb dating of sediments from soft-water lakes in New England (USA) and Scandinavia, a failure of
 774 ¹³⁷Cs dating. *Chemical Geology*, 44(1-3), 151-185.
- 775 DDEP – DATA DECAY EVALUATION PROJECT. LNELNHB/ CEA. (August 2010). Table de radionucléides
 776 ²¹⁰Pb. Retrieved from http://www.nucleide.org/DDEP_WG/DDEPdata.htm
- 777 Dillon, P., Scholer, P. and Evans, H. (1986). ²¹⁰Pb fluxes in acidified lakes. Sediments and water
 778 interactions (pp. 491-499) *Springer*.
- 779 Ecological Stratification Working Group (Canada), Center for Land, Biological Resources Research
 780 (Canada), & Canada. State of the Environment Directorate. (1996). A national ecological framework for
 781 Canada. Centre for Land and Biological Resources Research; Hull, Quebec: State of the Environment
 782 Directorate.
- 783 Ghaleb, B. (2009). Overview of the methods for the measurement and interpretation of short-lived
 784 radioisotopes and their limits. Paper presented at the IOP Conference Series: *Earth and Environmental*
 785 *Science*, 5(1) 012007.
- 786 Goldberg, E. (1963). Geochronology with ²¹⁰Pb radioactive dating. *International Atomic Energy Agency*,
 787 Vienna, 121, 130.
- 788 Jenny, J.P., Normandeau, A., Francus, P., Taranu, Z.E., Gregory-Eaves, I., Lapointe, F., Jautzy, J., Ojala,
 789 A.E., Dorioz, J.M., Schimmelmann, A. and Zolitschka, B. (2016). Urban point sources of nutrients were
 790 the leading cause for the historical spread of hypoxia across European lakes. *Proceedings of the National*
 791 *Academy of Sciences of the United States of America*, 113(45), 12655-12660.
 792 doi:10.1073/pnas.1605480113 [doi]
- 793 Klaminder, J., Appleby, P., Crook, P. and Renberg, I. (2012). Post-deposition diffusion of ¹³⁷Cs in lake
 794 sediment: Implications for radiocaesium dating. *Sedimentology*, 59(7), 2259-2267.
- 795 Koide, M., Soutar, A. and Goldberg, E. D. (1972). Marine geochronology with ²¹⁰Pb. *Earth and Planetary*
 796 *Science Letters*, 14(3), 442-446.

- 797 Korosi, J. B., Ginn, B. K., Cumming, B. F. and Smol, J. P. (2013). Establishing past environmental
 798 conditions and tracking long-term environmental change in the Canadian maritime provinces using lake
 799 sediments. *Environmental Reviews*, 21(1), 15-27.
- 800 Krishnaswami, S. and Lal, D. (1978). Radionuclide limnology. *Lakes* (pp. 153-177) Springer.
- 801 Last, W. M. and Smol, J. P. (2002). Tracking environmental change using lake sediments: Volume 2:
 802 Physical and geochemical methods *Springer Science & Business Media*.
- 803 Martz, D. E., Langner, G. H., Jr, and Johnson, P. R. (1991). Half-lives of ^{214}Pb and ^{214}Bi . *Health Physics*,
 804 61(4), 511-518. doi:10.1097/00004032-199110000-00006 [doi]
- 805 Millet, L., Giguët-Covex, C., Verneaux, V., Druart, J., Adatte, T. and Arnaud, F. (2010). Reconstruction of
 806 the recent history of a large deep prealpine lake (lake Bourget, France) using subfossil chironomids,
 807 diatoms, and organic matter analysis: Towards the definition of a lake-specific reference state. *Journal of*
 808 *Paleolimnology*, 44(4), 963-978.
- 809 Muggeo, V. M. R. (2003). Estimating regression models with unknown break-points. *Statistics in*
 810 *Medicine*, 22(19), 3055-3071. doi:10.1002/sim.1545
- 811 Openshaw, S. (1983). The modifiable areal unit problem. *Concepts and techniques in modern geography*
 812 38, GeoBooks, Norwich, England.
- 813 Pennington, W., Cambray, R., Eakins, J. and Harkness, D. (1976). Radionuclide dating of the recent
 814 sediments of Blelham Tarn. *Freshwater Biology*, 6(4), 317-331.
- 815 Rogers L.A., Schindler D.E., Lisi P.J., Holtgrieve G.W., Leavitt P.R., Bunting L., Finney B.P., Selbie D.T.,
 816 Chen G., Gregory-Eaves I., Lisac M.J. and Walsh P.B. (2013) Centennial-scale fluctuations and regional
 817 complexity characterize Pacific salmon population dynamics over the past five centuries. *Proceedings of*
 818 *the National Academy of Sciences of the United States of America*, 110: 1750-1755.
- 819 Sanchez-Cabeza, J. and Ruiz-Fernández, A. (2012). ^{210}Pb sediment radiochronology: An integrated
 820 formulation and classification of dating models. *Geochimica Et Cosmochimica Acta*, 82, 183-200.
- 821 Schallenberg, M., de Winton, M. D., Verburg, P., Kelly, D. J., Hamill, K. D. and Hamilton, D. P. (2013).
 822 Ecosystem services of lakes. *Ecosystem Services in New Zealand: Conditions and Trends*. Manaaki
 823 Whenua Press, Lincoln, New-Zealand 203-225.
- 824 Team, R. C. (2013). R: A language and environment for statistical computing.
- 825 Tomkins, J. D., Antoniades, D., Lamoureux, S. F. and Vincent, W. F. (2008). A simple and effective
 826 method for preserving the sediment–water interface of sediment cores during transport. *Journal of*
 827 *Paleolimnology*, 40(1), 577-582.
- 828 Tomkins, J. D., Lamoureux, S. F., Antoniades, D. and Vincent, W. F. (2009). Sedimentary pellets as an ice-
 829 cover proxy in a high arctic ice-covered lake. *Journal of Paleolimnology*, 41(1), 225-242.
- 830 Turner, L. and Delorme, L. (1996). Assessment of ^{210}Pb data from Canadian lakes using the CIC and CRS
 831 models. *Environmental Geology*, 28(2), 78-87.

- 832 Winegardner, A. K., Legendre, P., Beisner, B. E. and Gregory-Eaves, I. (2017). Diatom diversity patterns
833 over the past c. 150 years across the conterminous United States of America: Identifying mechanisms
834 behind beta diversity. *Global Ecology and Biogeography*, 26(11), 1303-1315.
- 835 Wood, S. (2012). Mgcv: Mixed GAM computation vehicle with GCV/AIC/REML smoothness estimation.
- 836 Wright, S., Howard, B., Strand, P., Nylén, T. and Sickel, M. (1999). Prediction of ¹³⁷Cs deposition from
837 atmospheric nuclear weapons tests within the Arctic. *Environmental Pollution*, 104(1), 131-143.